The cohesin subunit RAD21L functions in meiotic synapsis and exhibits sexual dimorphism in fertility

Yurema Herrán[1,7]**, Cristina Gutiérrez-Caballero**[1,7]**, Manuel Sánchez-Martín**[2]**, Teresa Hernández**[1]**, Alberto Viera**[3]**, José Luis Barbero**[4]**, Enrique de Álava**[1]**, Dirk G de Rooij**[5]**, José Ángel Suja**[3]**, Elena Llano**[1,6,]*** and Alberto M Pendás**[1,]***

[1]Instituto de Biología Molecular y Celular del Cáncer (CSIC–USAL), Campus Miguel de Unamuno S/N, Salamanca, Spain, [2]Departamento de Medicina, Campus Miguel de Unamuno S/N, Salamanca, Spain, [3]Unidad de Biología Celular, Universidad Autónoma de Madrid, Madrid, Spain, [4]Departamento de Proliferación Celular y Desarrollo, Centro de Investigaciones Biológicas (CSIC), Madrid, Spain, [5]Center for Reproductive Medicine, Academic Medical Center, University of Amsterdam, The Netherlands and [6]Departamento de Fisiología, Campus Miguel de Unamuno S/N, Salamanca, Spain

The cohesin complex is a ring-shaped proteinaceous structure that entraps the two sister chromatids after replication until the onset of anaphase when the ring is opened by proteolytic cleavage of its α-kleisin subunit (RAD21 at mitosis and REC8 at meiosis) by separase. RAD21L is a recently identified α-kleisin that is present from fish to mammals and biochemically interacts with the cohesin subunits SMC1, SMC3 and STAG3. RAD21L localizes along the axial elements of the synaptonemal complex of mouse meiocytes. However, its existence as a bona fide cohesin and its functional role awaits in vivo validation. Here, we show that male mice lacking RAD21L are defective in full synapsis of homologous chromosomes at meiotic prophase I, which provokes an arrest at zygotene and leads to total azoospermia and consequently infertility. In contrast, RAD21L-deficient females are fertile but develop an age-dependent sterility. Thus, our results provide in vivo evidence that RAD21L is essential for male fertility and in females for the maintenance of fertility during natural aging.

*Corresponding authors. E Llano or AM Pendás, Instituto de Biología Molecular y Celular del Cáncer (CSIC–USAL), Campus Miguel de Unamuno, 37007 Salamanca, Spain. Tel.: + 34 92 329 4809; Fax: + 34 92 329 4743; E-mail: ellano@usal.es or amp@usal.es
[7]These authors contributed equally to this work

Introduction

Structurally, the somatic cohesin complex consists of four subunits: two members of the family of proteins responsible for the structural maintenance of chromosome (SMC1α and SMC3) that heterodimerize, one kleisin subunit that closes the ring (Scc1/RAD21) and is the substrate for the protease separase, and a HEAT repeat domain protein (SA1/STAG1 or SA2/STAG2). In vertebrates, during prophase, most of the cohesins are dissociated from the chromatid arms by phosphorylation of the STAG1/2 subunit by PLK1 (polo-like-kinase 1) (Losada et al, 2002; Sumara et al, 2002). The remaining centromeric cohesins are released from chromosomes at the onset of anaphase by the cleavage of RAD21 by separase (Musacchio and Salmon, 2007).

During meiosis, two rounds of chromosome segregation follow a single round of replication to generate haploid gametes. The first meiotic division differs from mitosis in that homologous chromosomes pair, synapse, recombine and segregate to opposite poles as a result of their mono-orientation. The second meiotic division is similar to mitosis since the two recombined chromatids segregate to opposite poles (bi-orientation). During the onset of anaphase I, loss of sister chromatid arm cohesion occurs following separase-dependent cleavage of REC8, that replaces RAD21 during meiosis (Kudo et al, 2006, 2009). However, centromeric cohesion is maintained by the protective action of shugoshin-like-2 preventing separase-mediated cleavage of REC8 (Llano et al, 2008). This mechanism enables bi-orientation of recombined homologues. Once chromosomes have congressed at the metaphase II plate, separase is reactivated and centromeric cohesin complexes are released to allow chromatid segregation. In addition to REC8 (Parisi et al, 1999), a meiotic paralogue of RAD21, there are also meiosis-specific mammalian paralogues of SMC1α, and STAG1–2, that is SMC1β and STAG3, respectively (Prieto et al, 2001; Gruber et al, 2003).

Aside from these canonical functions, the cohesin complexes also participate in somatic homologous recombination between sister chromatids allowing the assembly of recombinational repair complexes, as well as recombination between homologous chromatids by assembly of the synaptonemal complex (SC) in meiocytes (Klein et al, 1999; Hartsuiker et al, 2001). The SC consists of a proteinaceous structure, the axial element (AE), allowing the association of each pair of sister chromatids. After pairing, the AEs are called lateral elements (LEs) to which transverse filaments (TFs) associate to give rise to the tripartite SCs. The SC provides the structural framework for synapsis, double-strand break (DSB) repair and exchange between homologues (Henderson and Keeney, 2005). During prophase I, most if not all, cohesin subunits expressed in mammalian spermatocytes colocalize with SYCP3, a structural AE/LE component (reviewed in Suja and Barbero, 2009). In fission and budding

yeast, the RAD21/Scc1 α-kleisin of the cohesin complex is replaced by the meiosis-specific REC8 protein. Yeast *rec8* mutants exhibit premature sister chromatid separation during prophase I, that are defective for the assembly of the SC (Klein *et al*, 1999). It has been assumed that most eukaryotes display a dual α-kleisin system (REC8 versus RAD21) similar to the well-studied system of *Schizosaccharomyces pombe* and *Saccharomyces cerevisae*, aside from the notable exception of *Caenorhabditis elegans* (Severson *et al*, 2009). Very recently, we and two other groups have biochemically characterized a new member of the α-kleisin family of proteins, RAD21L (Gutiérrez-Caballero *et al*, 2011; Ishiguro *et al*, 2011; Lee and Hirano, 2011). RAD21L, is a paralogue of RAD21 and it is transcribed more abundantly in testis and has been postulated to be a canonical cohesin subunit. RAD21L interacts with SMC3, SMC1α/β and STAG3 (Gutiérrez-Caballero *et al*, 2011; Ishiguro *et al*, 2011; Lee and Hirano, 2011). Consequently, the protein is localized to the AEs/LEs in meiocytes.

From the four meiotic-specific cohesins described (REC8, STAG3, SMC1β and RAD21L), loss of function mouse models for REC8 (Bannister *et al*, 2004; Xu *et al*, 2005) and SMC1β (Revenkova *et al*, 2004) have been developed. REC8 mutant male and female mice are sterile and show severe defects in synapsis, and chiasma formation (Bannister *et al*, 2004; Xu *et al*, 2005). SMC1β-deficient males show a pachytene arrest whereas mutant females present a premature loss of cohesion at metaphase II that leads to sterility (Revenkova *et al*, 2004).

In this work, we describe the precise localization of RAD21L in mouse spermatocytes and its functional characterization by a gene targeted mutation in the mouse. We provide cytological and *in vivo* evidence showing that the roles of RAD21L differ from those of RAD21 and REC8, and that RAD21L is as essential as REC8 for driving the initial steps of prophase I in male meiosis. RAD21L-deficient males show a defect in chromosome synapsis at prophase I, which provokes an arrest at a zygotene-like stage leading to total azoospermia. In contrast, RAD21L-deficient females are fertile but develop an age-dependent sterility. Thus, our results demonstrate for the first time that the recently identified RAD21L is a functionally relevant meiotic α-kleisin, which is essential for male fertility and for the maintenance of fertility during natural aging.

Results and discussion

Immunolocalization of the RAD21L protein
The recently identified third member of the α-kleisin protein family in mammals, RAD21L, is expressed in spermatocytes throughout meiosis I (Ishiguro *et al*, 2011; Lee and Hirano, 2011), with some discrepancies in relation with its time of disappearance (pachytene versus metaphase I). In order to assess the localization of RAD21L, we carried out a detailed analysis of mouse spermatocytes spreads using immunofluorescent (IF) antibodies. RAD21L was first detected at the leptotene stage as short threads that colocalized with SYCP3 along developing AEs (Figure 1A–D). During zygotene, RAD21L colocalized with SYCP3 at both the autosomal AEs/LEs, and the unsynapsed AEs of the sex chromosomes (Figure 1E–H). In early pachytene, RAD21L was detected as lines along the autosomal SCs where it colocalized with

SYCP3. Further signals for RAD21L were found at the pseudoautosomal region of homology between the sex chromosomes, where their AEs are synapsed. Furthermore, there was some additional staining in the unsynapsed AEs of the XY bivalent (Figure 1I and J). By late pachytene, there was an increase in RAD21L labelling on the sex chromosomal AEs and on the chromatin of the sex body (Figure 1K and L). This localization contrasts with the observed weak staining of REC8 at the AEs of the sex chromosomes at pachytene (see asterisks in Figure 7Q and R). In early diplotene, the intensity of the RAD21L labelling decreased along the desynapsing and still synapsed LEs (Figure 1M–P) to finally disappear by mid-diplotene (Figure 1Q and R). Concomitantly, RAD21L labelling began to accumulate at centromeres (Figure 1O–T) while it was progressively lost from the AEs and the chromatin of the sex chromosomes (Figure 1M–T). During diakinesis, RAD21L was highly enriched at the centromeres of all autosomes and was not detected along the desynapsed LEs. However, there was a faint RAD21L signal at the unsynapsed AEs of the sex chromosomes (Figure 2A and B). This pattern of RAD21L distribution remained during metaphase I (Figure 2C–F). At higher magnification, metaphase I autosomal bivalents show RAD21L signal at their centromeres but the labelling did not completely colocalize with SYCP3 at the inner centromere domain (ICD) (Figure 2G–I). With regards to the metaphase I sex bivalent, a faint RAD21L signal was observed along its interchromatid domain (Figure 2J). In addition, the centromeric RAD21L signal at the Y was larger than that at the centromere of the X chromosome (Figure 2J). The labelling of RAD21L was similar for both metaphase I and anaphase I (Figure 2F and K). During the second meiotic division, RAD21L was detected as a pair of brightly stained spots at the centromeres of metaphase II chromosomes (Figure 2L), and as single spots in segregating chromatids at anaphase II (Figure 2M).

Our results partially agree with those very recently reported on the distribution of RAD21L in mouse spermatocytes by Ishiguro *et al* (2011) and to a lesser extent with those reported by Hirano's group (Lee and Hirano, 2011). However, there are some differences with respect to the distribution pattern of RAD21L along the AEs/LEs. Besides the remarkable divergence in the timing of disappearance of RAD21L during meiosis I (pachytene versus metaphase I), these two groups described that RAD21L and REC8 localize as discontinuous (mutually exclusive) lines along zygotene AEs/LEs and pachytene SCs. Based on this, Ishiguro *et al* (2011) have proposed a cohesin 'barcode' model where meiosis-specific cohesin complexes with either RAD21L or REC8 have intrinsic and alternating loading sites along the AEs/LEs, which might facilitate homologous pairing. However, our antibodies detected continuous lines along SCs. These discrepancies might be due to differences in image acquisition, different sensitivity of the antibodies used, or dilutions employed. This aspect will need further clarification.

The three kinds of cohesin complexes comprised of RAD21, RAD21L or REC8 might have different functions during both meiotic divisions since their distribution and dynamics are different not only during prophase I, but also during metaphase I and metaphase II. For instance, in metaphase II chromosomes, RAD21L appears as two separate signals at each centromere (Figure 2L), which is in contrast to RAD21 that has not been detected at centromeres (Parra *et al*,
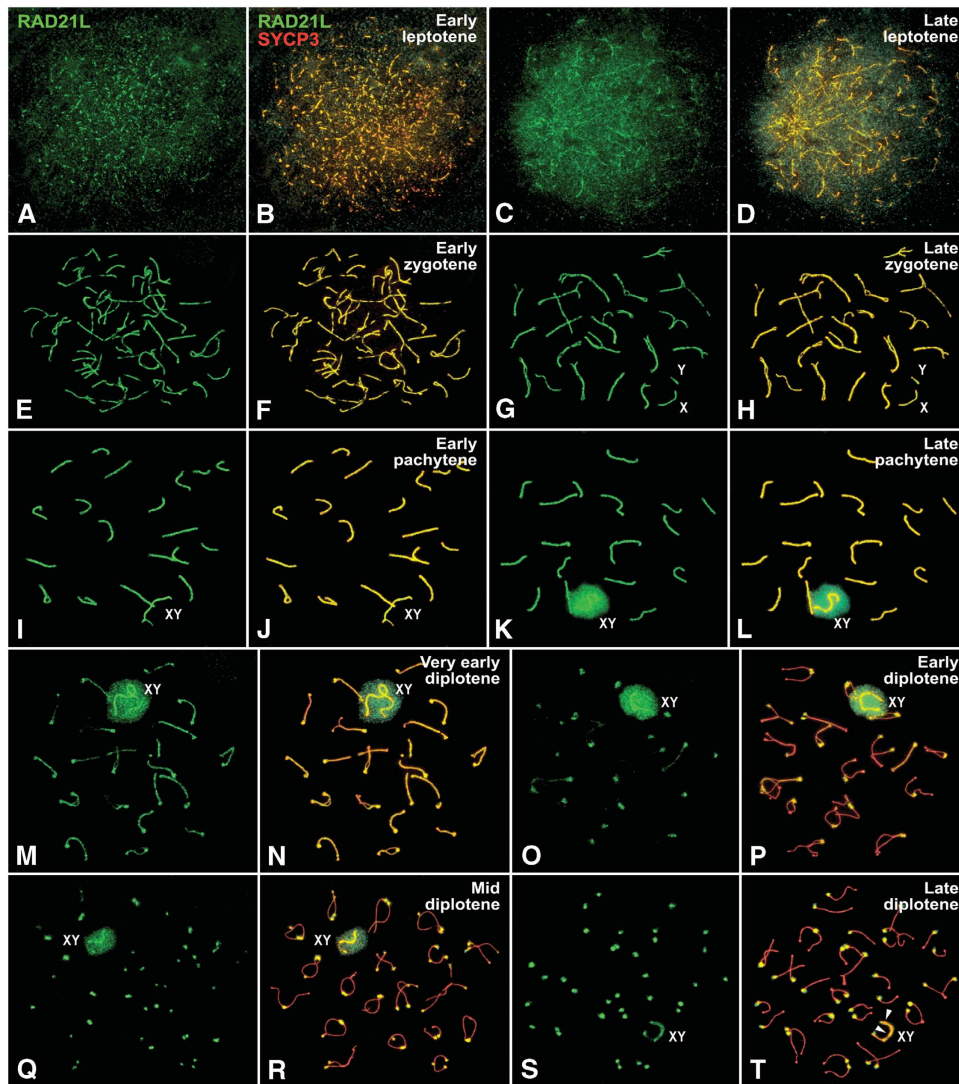
Figure 1 Distribution of RAD21L during prophase I. Double immunolabelling of RAD21L (green) and SYCP3 (red) in spread spermatocytes. (**A–D**) During leptotene, RAD21L appears as a succession of small dots that colocalize with SYCP3 along developing AEs. (**E–H**) During zygotene, RAD21L and SYCP3 colocalize along AEs/LEs. Sex chromosomes (X, Y) have still not synapsed. (**I–L**) RAD21L colocalizes with SYCP3 along autosomal SCs and sex chromosomes (XY) AEs. In late pachytene (**K, L**), RAD21L appears enriched at the chromatin of the sex body (XY) and at their AEs. (**M–P**) In early diplotene, RAD21L vanishes along desynapsing autosomal LEs, but is still enriched at the sex AEs and at the sex body (XY). (**Q–T**) In mid and late diplotene, RAD21L appears at the centromeres and along the sex AEs, and faintly at the sex body (XY).

2004), while REC8 appears at the ICD as one spot between sister kinetochores consistent with its role in centromere cohesion (Kudo *et al*, 2006). While the distribution of REC8 is consistent with its function in maintaining both arm and centromere cohesion during the two meiotic divisions (Kudo *et al*, 2006, 2009; Tachibana-Konwalski *et al*, 2010), the localization of RAD21 and RAD21L suggests that they might have different roles. In this regard, the accumulation of RAD21L at centromeres during diplotene, its enrichment at the centromere of the Y chromosome during metaphase I, and its distribution at metaphase II centromeres is strikingly similar to the distribution of the shugoshin-like-2 (Gómez *et al*, 2007; Llano *et al*, 2008) and MCAK (Parra *et al*, 2006) during male mouse meiosis. Thus, the enrichment of RAD21L at centromeres during diplotene might contribute to the assembly of the ICD (Parra *et al*, 2009).

Gene disruption of Rad21l

To address the function of RAD21L and to validate genetically that it constitutes a functional subunit of a novel meiotic cohesin, we created a targeted mutation of the murine *Rad21l* locus by an insertional strategy that disrupts the open reading frame (ORF) of the locus (Supplementary Figure S1A and B; Adams *et al*, 2004). Heterozygous targeted mice transmitted the mutation to the offspring at Mendelian frequencies (1:2:1). RT–PCR was used to evaluate the interruption of the ORF of the *Rad21l* gene in the homozygous targeted mice (Supplementary Figure S1C; see Materials and methods). The absence of the protein in these homozygous targeted mice was also validated using two different antibodies, which were specific against RAD21L (Supplementary Figures S1E and S2; Gutiérrez-Caballero *et al*, 2011). Consequently, spermatocytes from homozygous targeted mice did not show RAD21L immunofluorescence (Supplementary Figure S1D).
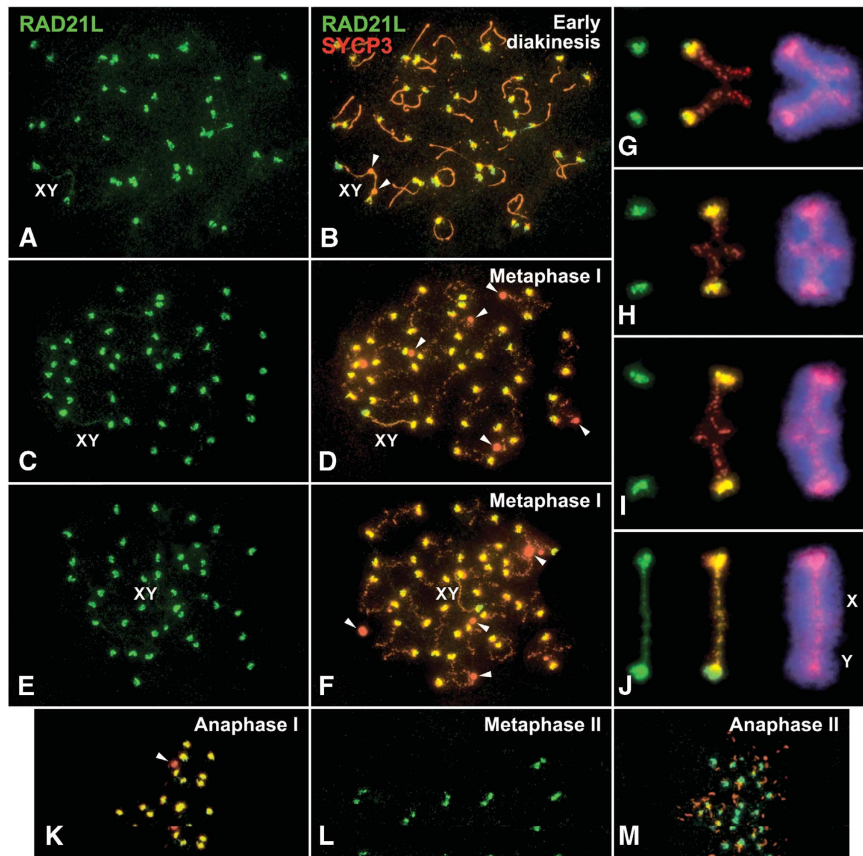
Figure 2 Distribution of RAD21L during diakinesis and meiotic divisions. Double immunolabelling of RAD21L (green) and SYCP3 (red) and counterstaining of chromatin with DAPI (blue) in spread spermatocytes. (**A–F**) During early diakinesis (**A**, **B**) and metaphase I (**C–F**), RAD21L is present at the centromeres of all chromosomes and at the interchromatid domain of the sex bivalent (XY). Arrowheads mark the enlargements of SYCP3 along the X chromosome in diakinesis, and the large agglomerates of SYCP3 in the cytoplasm of metaphase I spermatocytes. (**G–I**) Enlargements of three selected metaphase I bivalents. RAD21L is enriched at the centromeres but does not completely localize with SYCP3, and is not present at the interchromatid domain where SYCP3 is detected. (**J**) Selected metaphase I sex bivalent. RAD21L appears as a faint signal along the interchromatid domain and as bright signals at the centromeres. The RAD21L signal at the centromere of the Y chromosome (Y) is larger than that present at the X chromosome (X). (**K**) RAD21L partially colocalizes with SYCP3 at anaphase I centromeres. Arrowhead marks an SYCP3 agglomerate. (**L**, **M**) RAD21L appears as a pair of signals at metaphase II centromeres (**L**) and as single signals at anaphase II centromeres (**M**).

Heterozygous targeted mice showed neither cellular nor aberrant organismal phenotypes (indicative of the lack of a gain of function). Thus, we concluded that the mutation is functionally a null allele of *Rad21l*.

Histological analysis and male infertility in Rad21l$^{-/-}$ mice

Rad21l$^{-/-}$ mice developed normally and displayed no overt phenotype. However, while female mice lacking RAD21L were fertile, males were sterile since they failed to produce offspring. Testes from *Rad21l*$^{-/-}$ mice were on average 70% smaller than those from wild-type mice, and their epididymides lacked spermatozoa (Figure 3A and B). Histopathological analysis revealed an absence of postmeiotic cell types despite of the presence of spermatogonia, and Sertoli and Leydig cells (Figure 3A). Within a mouse testis, the seminiferous epithelium contains a mixture of germ cells at various developmental stages. Staging of each tubule section is defined (from I to XII) according to the group of associated germ cell types that are present (Russell, 1990). Following this criteria, mutant mice appeared to be arrested at stage IV of the epithelial cycle (Figure 3A). FACS analysis of whole cells from seminiferous tubules was carried out and

sustained the prophase I arrest by the absence of the haploid compartment in *Rad21l*$^{-/-}$ testes (Figure 3B). In order to rule out proliferation defects in spermatogonia, PCNA immuno-staining of wild-type and *Rad21l*$^{-/-}$ tubules was performed and no differences in the basal layer of PCNA-positive cells were found (Figure 3C). Given the lack of spermatozoa, we carried out TUNEL staining and showed that the prevalence of apoptotic cells in *Rad21l*$^{-/-}$ tubules was higher than in wild type (Figure 3C). Finally, studying the histology of the testis, it became clear that spermatogenesis proceeds apparently normal up to prophase I. Then, in stage IV, there is a massive apoptosis of spermatocytes. Extensive apoptosis was also observed at 19 days of age (Figure 3D), indicating that spermatocytes of the first wave of spermatogenesis were already affected. Thus, we conclude that RAD21L is essential for spermatogenesis in the mouse and its deficiency provokes total azoospermia that leads to infertility.

SC morphology and synapsis in mutant spermatocytes
To functionally analyse the infertility in the mutant mice and to more precisely characterize the meiotic arrest, we first studied the assembly of the SC. Spermatocytes spreads were studied and staged by staining for SYCP3. It appeared that in
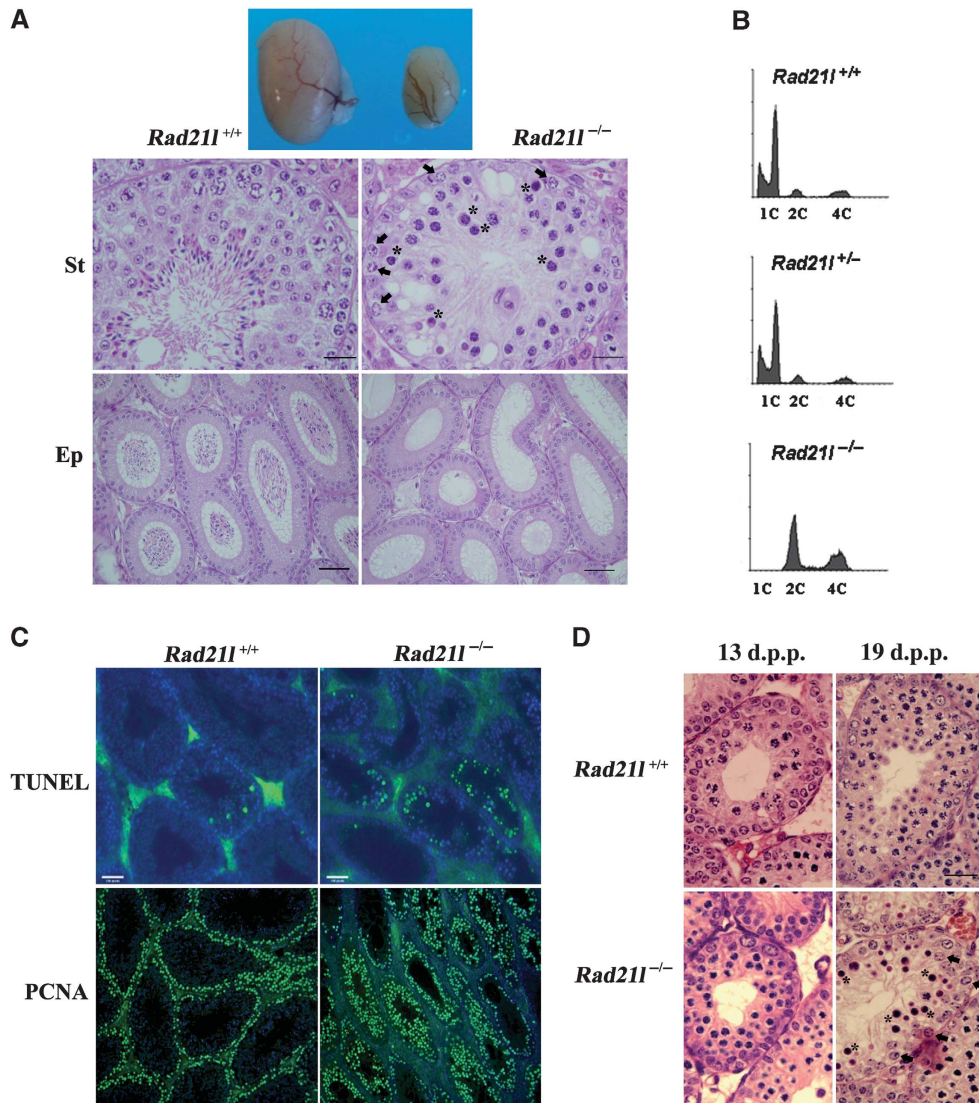
Figure 3 The absence of RAD21L provokes azoospermia. (**A**) The deficiency of RAD21L promotes a complete block of mouse spermatogenesis. Genetic ablation of *Rad21l* leads to a reduction of the testis size, and an arrest of spermatogenesis in epithelial stage IV, identified by the presence of intermediate spermatogonia (arrows) about to divide into B spermatogonia. Massive apoptosis of spermatocytes (asterisks) can be seen. The spermatogenic arrest leads to empty epididymides and azoospermia. Bar in upper panels, 100 μm and in lower panels, 25 μm. (St) Seminiferous tubules. (Ep) Epididymides. (**B**) Abnormal ploidy of *Rad21l*$^{-/-}$ spermatocytes. FACS analysis of cells from seminiferous tubules showing the absence of the haploid compartment in *Rad21l*$^{-/-}$ testes. (**C**) Immunohistochemical detection of proliferating cells with anti-PCNA and apoptotic cells by TUNEL staining show the absence of proliferative defects and an increase of apoptotic cells in *Rad21l*$^{-/-}$ seminiferous tubules, respectively. Bar in both panels, 25 μm. (**D**) Tubule degeneration in juvenile mice (13 days postpartum (d.p.p.) and 19 d.p.p.) lacking RAD21L and spermatogenic arrest prior to pachytene studied by histology of testes from *Rad21l*$^{+/+}$ and *Rad21l*$^{-/-}$ males. At 13 d.p.p., spermatogenesis has reached to late zygotene and at 19 d.p.p. to late pachytene. Spermatocyte apoptosis (asterisks) was first seen in 19 d.p.p.

the absence of RAD21L, synapsis between homologues was not completed (Figure 4A and B). To determine the extent of the disruption of synapsis, we monitored the distribution of the TF protein SYCP1 as colabelling of SYCP3 and SYCP1 highlights regions of synapsis in wild types. Mutant spermatocytes did not proceed beyond zygotene-like stage (Figure 4A). This blockade was further supported by the absence of immunolabelling for the mid-pachytene-specific histone variant H1T (Supplementary Figure S3), supporting the observed arrest at epithelial stage IV as determined by histological analysis (Figure 3A). Using SYCP3 staining of the zygotene-like spermatocytes from *Rad21l*$^{-/-}$ mice, we observed discontinuous/fragmented stretches of AEs that did not progress to the expected 19 fully synapsed autosomal bivalent chromosomes (Figure 4A and B). Furthermore, a

fraction of the arrested spermatocytes displayed ring-like structures (Figure 4B, arrowhead) and synapsis between non-homologous chromosomes occurred (Figure 4A and B, arrows). To further analyse the synaptic defects, we investigated the centromere distribution by immunolabelling with a human anti-centromere antibody (ACA) (Figure 4B). In wild-type leptotene spermatocytes, the number of centromere signals never exceeded 40. As synapsis progressed, these centromeric foci diminished to 21 (19 signals from synapsed autosomes + 2 signals of the XY bivalent) at pachytene when homologous pairing of autosomes is complete and their centromeres are very closely juxtaposed (Figure 4B). In *Rad21l*$^{-/-}$ zygotene-like spermatocytes, we scored on average 30 ± 3.5 foci (30 nuclei analysed). This result also points to a deficient synapsis between homologues, at least at
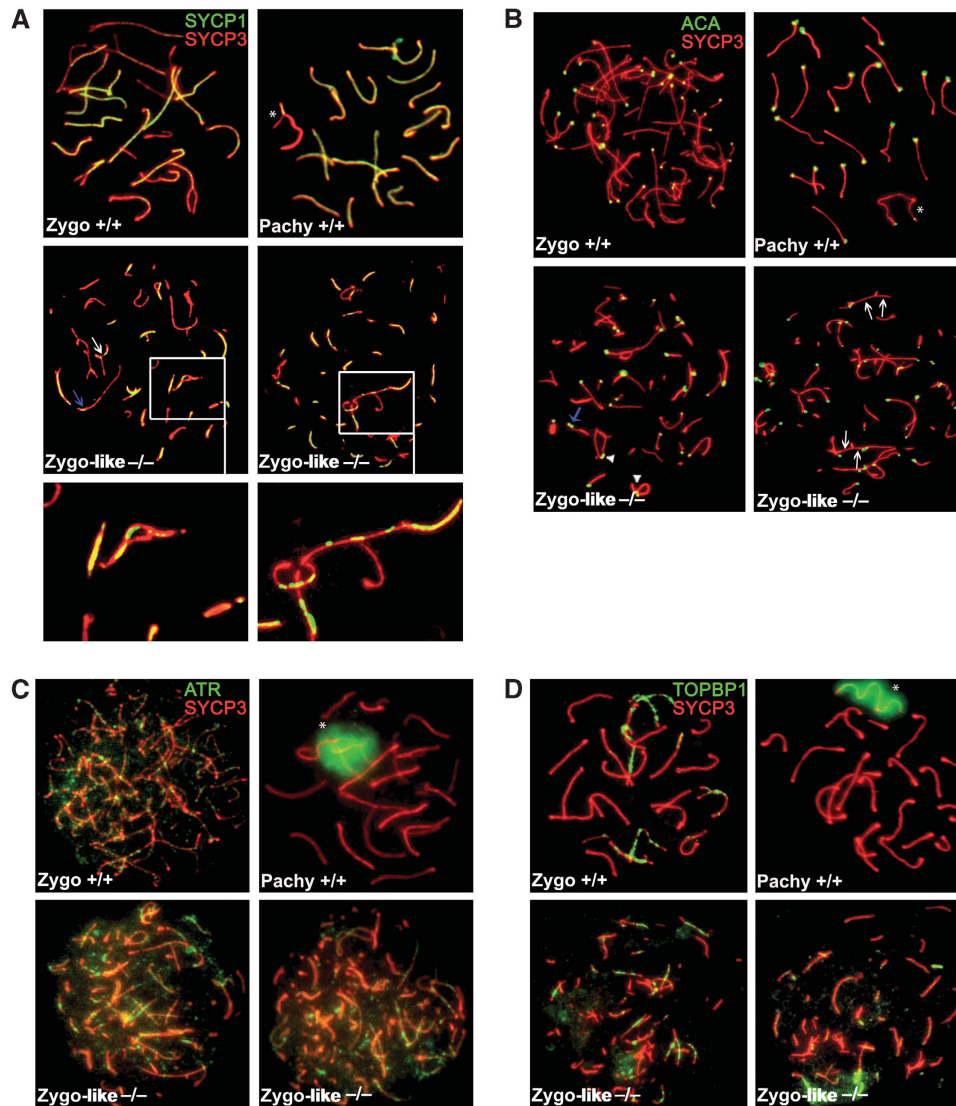
Figure 4 $Rad21l^{-/-}$ spermatocytes show defects in synapsis. (**A**) Double labelling of SYCP3 (red) and SYCP1 (green) showing fragmented AEs/LEs with aberrant synapsis and with patches of SYCP1 in mutant spermatocytes (arrow) as compared with their wild-type control. (**B**) Double immunolabelling of SYCP3 (red) and kinetochores (anti-centromere autoantibody, ACA (green)) in $Rad21l^{+/+}$ and $Rad21l^{-/-}$ spermatocytes. In wild-type spermatocytes, the number of ACA signals is reduced from 40 to 21 between zygotene to pachytene stage. These signals localize at one end of the AEs/SCs. In $Rad21l^{-/-}$ spermatocytes, synapsis is incomplete and the number of ACA signals is always higher than 21. The presence of some centromeres along the same synapsed region (blue arrow), some unsynapsed AEs between synapsed regions (arrow) and the presence of ring structures formed by chromosomes with two neighbouring centromeres (arrowhead) are indicatives of non-homologous synapsis. (**C**, **D**) Double immunolabelling of SYCP3 (red) and ATR or TOPBP1 (green) in wild-type or $Rad21l^{-/-}$ spermatocytes. In wild-type spermatocytes, ATR (**C**) and TOPBP1 (**D**) proteins localize to unsynapsed AEs. At pachytene, these proteins only appear at the sex body. In $Rad21l^{-/-}$ zygotene-like spermatocytes, these proteins remain accumulated at AEs. *Sex body (XY).

their centromeric regions (Figure 4B). In order to further study this failure of synapsis, we stained spermatocytes for the kinase ATR and the DNA-binding protein TOPBP1 as these reliably stain the unsynapsed AEs/LEs at leptotene–zygotene and the unsynapsed AEs and the chromatin of the sex body at pachytene (Perera *et al*, 2004). Moreover, TOPBP1 and ATR also accumulate at the unsynapsed AEs of mutant spermatocytes with a meiotic arrest such as $Dmc1^{-/-}$ and $Msh5^{-/-}$ spermatocytes (Barchi *et al*, 2005). Our immunolabelling results on wild-type spermatocytes revealed that ATR and TOPBP1 appeared as foci along the unsynapsed leptotene and zygotene AEs/LEs, whereas at mid-pachytene both proteins were restricted to the sex body (Figure 4C and D). RAD21L-deficient and wild-type spermatocytes showed a similar

number of ATR and TOPBP1 foci at leptotene and zygotene AEs. However, as meiosis arrested at a zygotene-like stage in $Rad21l^{-/-}$, these foci also persisted and were not eliminated (Figure 4C and D). In summary, RAD21L deficiency in mouse spermatocytes leads to abnormal AEs/LEs, which are fragmented and poorly aligned/synapsed (a large number of AEs are kept individually), some stretches of AEs and LEs are decorated with SYCP1 and synapsis between non-homologous chromosomes occurs.

Defective DSB processing in the mutant spermatocytes

The absence of REC8 leads to severe defects in DSB processing in yeast and to a lesser extent in mouse meiosis (Klein *et al*, 1999; Xu *et al*, 2005). Taking into account these data
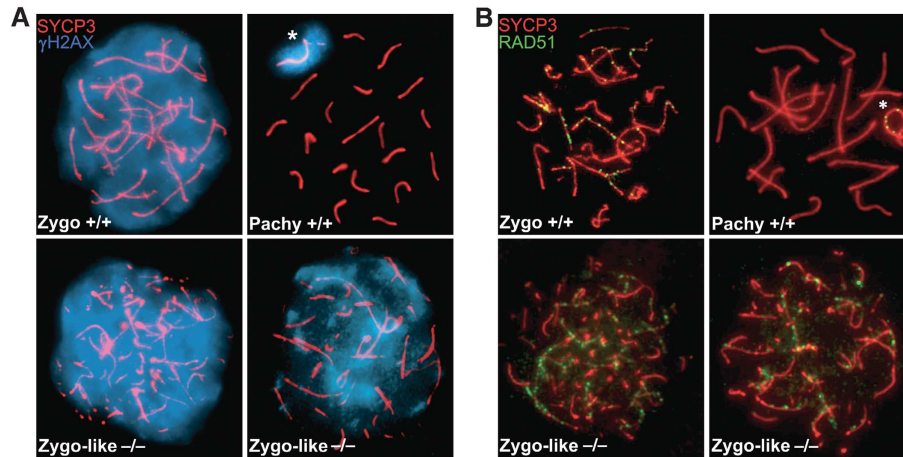
Figure 5 DSB-associated proteins in *Rad21l*$^{-/-}$ spermatocytes. (**A**, **B**) Double immunolabelling of SYCP3 (red) with γ-H2AX (blue) and RAD51 (green) in wild-type and *Rad21l*$^{-/-}$ spermatocytes. In wild-type zygotenes, γ-H2AX (**A**) labels the chromatin and RAD51 (**B**) labels multiple foci on the AEs/LEs. At wild-type pachytene, γ-H2AX labelling is reduced to the sex body and RAD51 foci are restricted to the XY bivalent. In RAD21L-deficient spermatocytes, γ-H2AX (**A**) and RAD51 (**B**) labelling is sustained in the zygotene-like-arrested spermatocytes. *Sex body (XY).

and the arrest observed in the *Rad21l* mutant, we studied whether RAD21L deficiency promotes a deficit in the repair of the programmed DSBs generated by the nuclease SPO11 at early leptotene, a frequent cause of meiotic arrest (Viera *et al*, 2009). Thus, we first monitored the formation of DSBs and analysed the presence of γ-H2AX histone variant, which is phosphorylated at prophase I in response to the SPO11-induced DSBs in an ATM-dependent manner. At zygotene, γ-H2AX labelling was equally strong in both *Rad21l*$^{-/-}$ and *Rad21l*$^{+/+}$ spermatocytes (Figure 5A). As pairing proceeds, γ-H2AX staining diminished in wild-type pachytene spermatocytes and appeared mainly at the chromatin of the sex body (Figure 5A). However, in *Rad21l*$^{-/-}$ spermatocytes arrested at a zygotene-like stage, the γ-H2AX labelling remained in the chromatin of synapsed and unsynapsed chromosomes, although this staining was reduced when compared with an earlier zygotene-like stage (Figure 5A). This result suggests an accumulation of unrepaired DSBs and/or asynapsis in *Rad21l*$^{-/-}$-arrested spermatocytes.

We next analysed the kinetics of proteins involved in this DSB-induced signalling cascade. After DSBs are induced, RAD51 is recruited to these early recombination nodules, which promotes homologous strand invasion (Mimitou and Symington, 2009). In wild-type zygotene spermatocytes, RAD51 assembles on the AEs/LEs of bivalents and disappears towards pachytene, with the exception of the unsynapsed sex AEs (Figure 5B). In *Rad21l*$^{-/-}$ zygotene-like spermatocytes, RAD51 immunolabelling was similar to wild-type zygotene controls (Figure 5B). These results suggest that RAD51 nodules are sustained in mutant spermatocytes either because RAD21L is required for their resolution or because meiotic progression arrests before the stage at which this process take place because of the synapsis defects.

Subsequently, we determined the distribution of the replication protein A (RPA) in RAD21L-deficient spermatocytes. RPA is a single-strand DNA-binding protein that interacts with RAD51 during the strand exchange and appears after RAD51 at the AEs/LEs (Moens *et al*, 2007). We observed a large number of RPA foci in both *Rad21l*$^{-/-}$ and wild-type zygotene spermatocytes (Supplementary Figure S4A). In wild-type

pachytene spermatocytes, RPA foci were present mainly over the synapsed LEs of the autosomes and more abundantly along the pseudoautosomal region of the sex chromosomes. In RAD21L-deficient zygotene-like spermatocytes, the RPA foci were mainly present at the LEs similar to wild-type zygotene controls (Supplementary Figure S4A).

Finally, we analysed the presence of MLH1 foci in mutant spermatocytes. MLH1 is a component of the postreplicative mismatch repair system and the number of its foci during pachytene matches those of chiasmata (Moens *et al*, 2007). MLH1 foci were absent in *Rad21l*$^{-/-}$ zygotene-like nuclei (Figure 6A), while one/two MLH1 foci per bivalent were observed in wild-type pachytene nuclei. Based on these results, we studied the recombination intermediary protein MSH4 since it mediates the transition from the initial recombination proteins RPA to MLH1 (Santucci-Darmanin *et al*, 2000). In *Rad21l*$^{-/-}$ zygotene-like spermatocytes, MSH4 signal was slightly decreased to that found in wild-type controls (Supplementary Figure S4B), suggesting that early/intermediate steps of recombination might be already altered in RAD21L null spermatocytes.

Okadaic acid-induced metaphase I-like spermatocytes

We further investigated whether crossing over (CO) and chiasmata could be formed in the absence of the meiotic arrest that precludes the *Rad21l*$^{-/-}$ spermatocytes to enter into pachytene, as well as the involvement of RAD21L in centromeric cohesion. To this end, we exposed the mutant spermatocytes to the PP2A inhibitor okadaic acid (OA), to allow *in vitro* transition from pachytene to metaphase I (Wiltshire *et al*, 1995). After OA treatment of wild-type spermatocytes, there was a rapid induction of SC disassembly, bivalent separation and chiasmata formation, which does not affect centromere cohesion. Treated wild-type spermatocytes revealed 20 bivalents, positive for SYCP3 immunolabelling at the interchromatid and centromeric domain, with two pairs of unseparated sister kinetochores, which were stained with ACA serum, and at least one chiasma (Figure 6Ba–c). In contrast, OA-treated *Rad21l*$^{-/-}$ spermatocytes displayed 40 unattached univalents with a characteristic labelling for
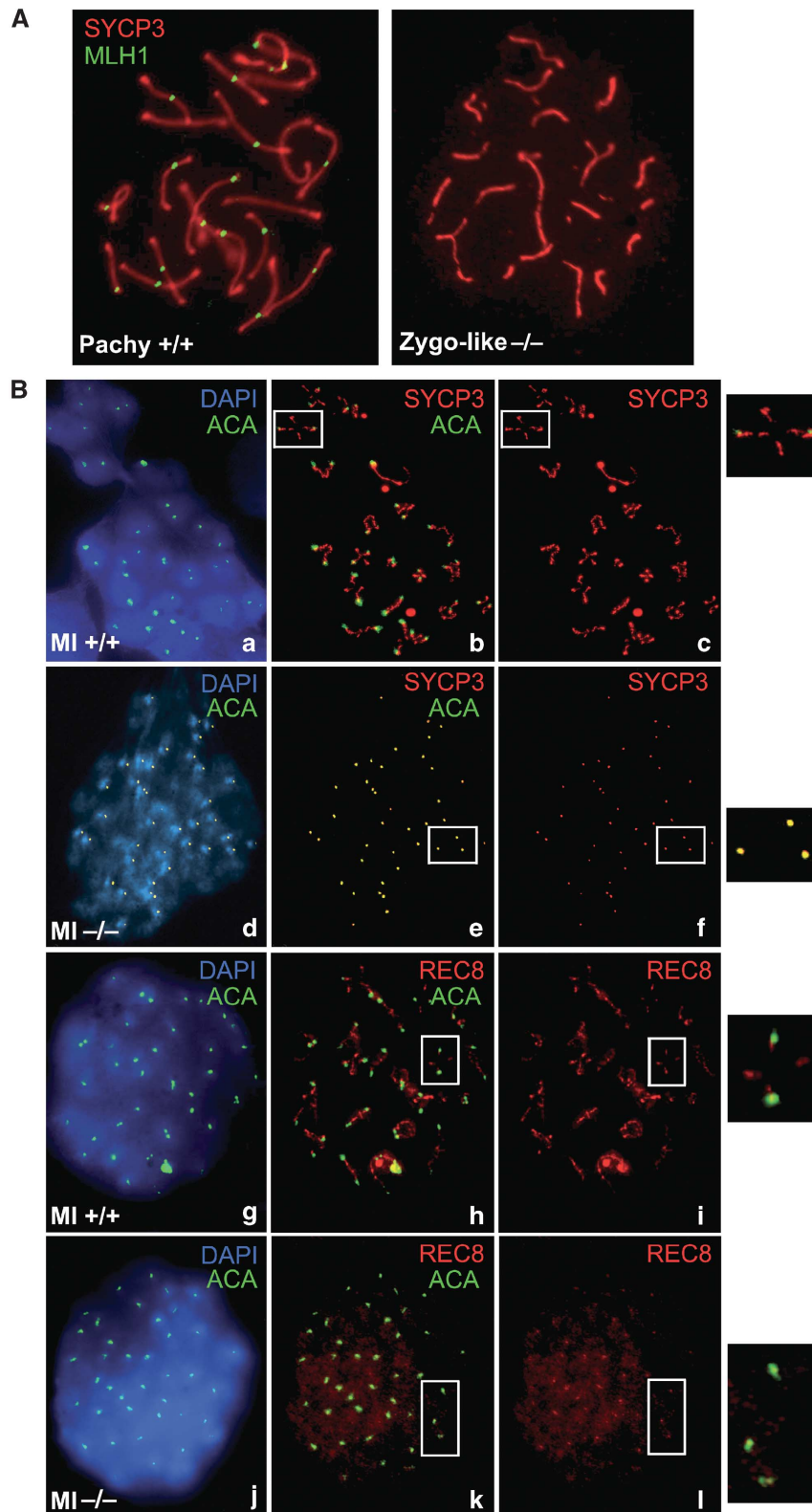
Figure 6 The deficiency of RAD21L prevents CO and does not affect centromeric cohesion. (**A**) Double immunolabelling of SYCP3 (red) with MLH1 (green). MLH1 foci are absent at the AEs/LEs of *Rad21l*$^{-/-}$ spermatocytes whereas at least one focus is present along each autosomal SC in wild-type pachytene spermatocytes. (**B**) Double immunolabelling of SYCP3 or REC8 (red) with ACA (green) and DAPI (blue) in wild-type and *Rad21l*$^{-/-}$ spermatocytes. OA-induced metaphase I plates of wild-type spermatocytes give rise to 20 bivalents each with two opposed centromere signals (**Ba–Bc, Bg–Bi**), whereas *Rad21l*$^{-/-}$ spermatocytes lead to 40 separated centromere signals (**Bd–Bf, Bj–Bl**). The absence of spermatocytes with >40 independent signals of ACA (**Bd–Bf**) and REC8 (**Bj–Bl**) revealed the preservation of the centromeric cohesion in the absence of RAD21L. Islets represent magnification of one wild-type bivalent and some *Rad21l*$^{-/-}$ unjoined chromosomes.

SYCP3 only at the centromeric domain (Figure 6Bd–f) (20 cells per individual; 3 individuals from each genotype). To further demonstrate that centromeric cohesion was not affected by the absence of RAD21L, we stained these pseudometaphases with REC8 and ACA and showed that REC8 staining persisted at centromeres in metaphase I-like spermatocytes from *Rad21l*$^{-/-}$ mice (Figure 6Bj–l). Altogether, these results reveal that the DSBs can start as part of the meiotic recombination programme in the absence of RAD21L, but they are not processed appropriately and accumulate in an intermediate unrepaired state before reciprocal recombination and CO take place. The observation of 40 rather than 80 centromere signals associated with separated chromatids is indicative of the persistence of centromeric cohesion. These results are in agreement with the apparent release of RAD21L from the desynapsed LEs at diplotene, whereas RAD21 and REC8 persist and do not relocate to centromeres (Eijpe *et al*, 2003; Parra *et al*, 2004), suggesting that RAD21L-containing cohesin complexes are not required for maintaining sister chromatid arm cohesion from diplotene up to the metaphase I/anaphase I transition. These results, together with the preferential localization of RAD21L at the sex chromosomal AEs at the expense of REC8 (Figure 7Q and R), make it tempting to speculate that RAD21L is involved in the arrangement of specific cohesin complexes that despite not participating in arm chromosome cohesion have important roles in the assembly of the SC, progression of synapsis and recombination and in sex body formation in spermatocytes.

In *Smc1β*$^{-/-}$ mice, metaphase II chromosomes from oocytes and metaphase I OA-induced chromosomes from spermatocytes are defective in centromere cohesion (Revenkova *et al*, 2004). This chromosomal phenotype has not been analysed in *Rec8* mutant mice since males (in the absence of OA experiments) and females show a premature arrest prior to pachytene due to a lack of full homologous synapsis. However, it is widely assumed that REC8 is the essential kleisin involved in chromosome cohesion in meiosis I and II based on the phenotype of *Rec8* null mutant models in several species (Klein *et al*, 1999; Bannister *et al*, 2004; Xu *et al*, 2005; Severson *et al*, 2009). This is also confirmed using genetically modified mice with mutations in the *Rec8* gene (Kudo *et al*, 2009; Tachibana-Konwalski *et al*, 2010). Although the OA-induced chromosomes from *Rad21l*$^{-/-}$ spermatocytes do not fully resemble metaphase I stage with a functional meiotic spindle, the maintenance of centromeric cohesion under these experimental conditions in *Rad21l* mutant spermatocytes (Figure 6Bd–f and Bj–l), together with the cytological localization of RAD21L in metaphase I and II (Figure 2D, F and L), indicates that RAD21L is not involved in chromosome cohesion in males. Thus, and although not strictly demonstrated in all of these experimental models, it is very likely that the only α-kleisin supporting chromosome cohesion in mammalian meiosis is REC8 by forming a cohesin complex with SMC3, SMC1β and STAG3.

Cohesion complexes in mutant spermatocytes

RAD21L has recently shown to be a component of the cohesin complex together with SMC1α/β, SMC3 and STAG3 (Gutiérrez-Caballero *et al*, 2011; Ishiguro *et al*, 2011; Lee and Hirano, 2011). Therefore, also considering the stoichiometric relationship of each subunit within a cohesin complex, the genetic ablation of RAD21L could alter the loading at the cohesin axis of other subunits. We thus undertook a direct analysis of the presence of different cohesin subunits in the absence of RAD21L. There was no substantial variation in the loading of REC8, SMC1β, RAD21 or SMC3 along the cohesin axis at the AEs/LEs in mutant zygotene-like spermatocytes (Figure 7F, N, P and V). However, the existence of STAG3, and to a lesser extent SMC1α, was partially reduced from leptotene to zygotene-like arrest when compared with wild-type spermatocytes (Supplementary Figures S5 and S6; Figure 7H and X). In mouse testis extracts, it has been shown by immunoprecipitation analysis that STAG3 associates with the three α-kleisins (Ishiguro *et al*, 2011; Lee and Hirano, 2011). We now provide *in vivo* evidence that lack of RAD21L is sufficient to promote a partial loss of STAG3 from the AEs/LEs. Overall, these data show that RAD21L is interacting *in vivo* with STAG3, leading to a functional and meiosis-specific cohesin complex, together with SMC3 and SMC1, that is essential for the synapsis of homologous chromosomes.

From a more functional point of view, STAG3 is normally assembled in the AEs/LEs of REC8-deficient spermatocytes (Bannister *et al*, 2004). Taken together, and given the impossibility to analyse spermatocytes in *Rad21*$^{-/-}$ mice due to their embryonic lethality (Xu *et al*, 2010), these results strongly suggest that RAD21L is quantitatively an important α-kleisin involved in STAG3 complexing.

Telomere behaviour in mutant spermatocytes

The formation of a cluster of telomeres very early during meiotic prophase is important for accurate pairing and recombination (Scherthan, 2001). Mice deficient for the cohesin SMC1β show an incomplete attachment of telomeres to the nuclear envelope (Adelfalk *et al*, 2009). We therefore investigated telomere distribution in RAD21L-deficient spermatocytes. We analysed this feature on squashed spermatocytes to preserve the separation of peripheral and internal nuclear domains. While in wild-type pachytene spermatocytes, all telomeric signals were close to the nuclear envelope (Supplementary Figure S7Aa), in *Rad21l*$^{-/-}$ zygotene-like spermatocytes some telomeric signals (from 1 to 6) appeared within the nucleus (Supplementary Figure S7Ab and c and B). These results indicate that in the absence of RAD21L, the attachment of telomeres to the nuclear envelope is partially misregulated.

The function of SMC1β in telomere protection rather than its role in AE assembly may be responsible for defective bouquet formation (Adelfalk *et al*, 2009). It is unclear whether the mild telomere disorganization observed is due to the general reduction of functional cohesin complexes caused by the loss of the subset of cohesin complexes containing RAD21L or due to the lack of RAD21L, specifically.

Meiosis in mutant female mice

In contrast to RAD21L-deficient males, *Rad21l*$^{-/-}$ females were fertile up to 6 months of age and generated healthy offspring with litter sizes similar to wild-type females. However, the mutant females exhibited premature onset of subfertility around this age, showing on average 5.2 pups per litter compared with 8.9 in wild-type females. Around 10 months of age, *Rad21l*$^{-/-}$ females became sterile, whereas their wild-type counterparts remained fertile. To analyse the underlying loss of fertility with age, we conducted IF and
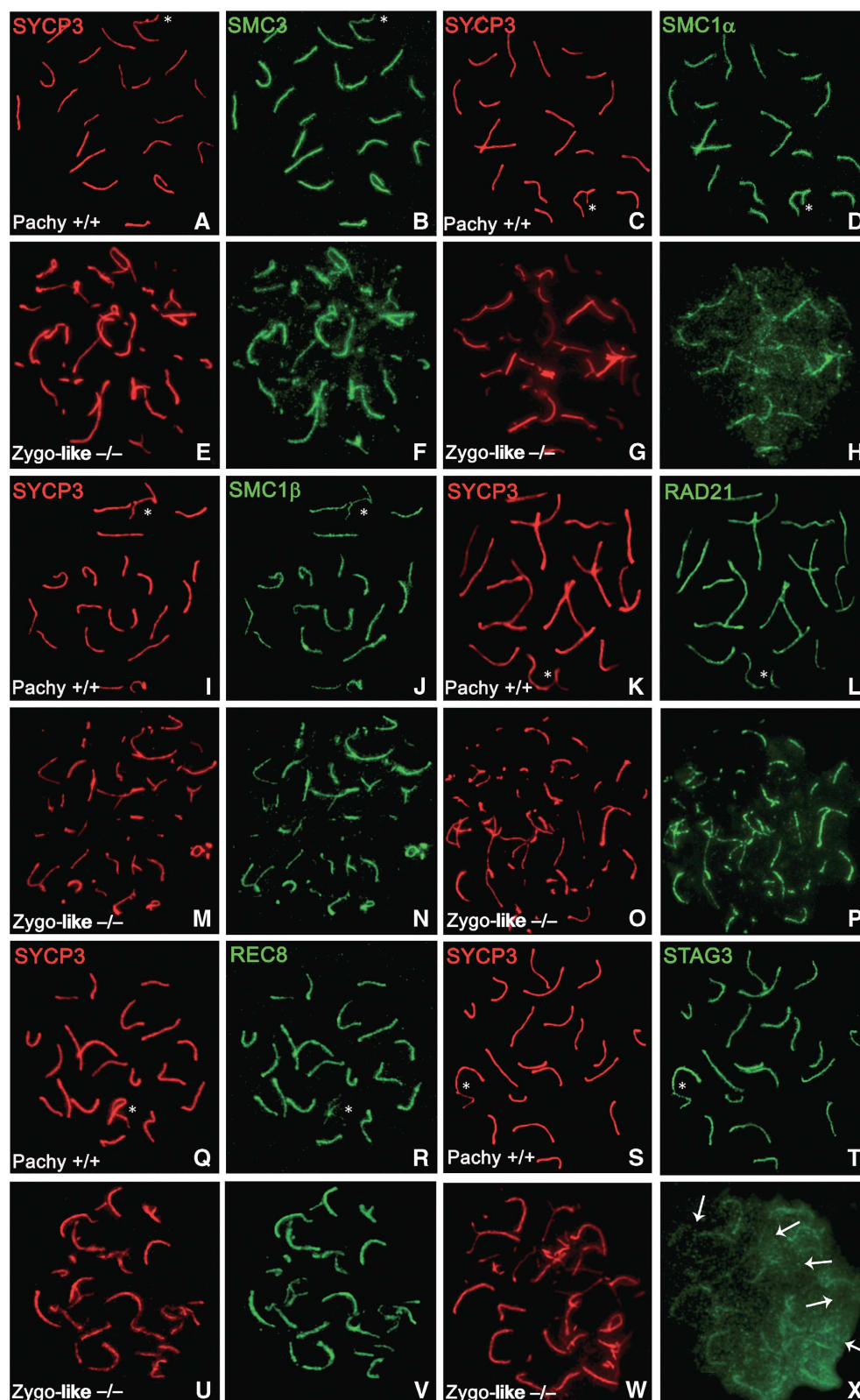
Figure 7 Immunolabelling of the cohesin subunits SMC3, SMC1α, SMC1β, RAD21, REC8 and STAG3 in *Rad21l*$^{+/+}$ and *Rad21l*$^{-/-}$ spermatocytes. Double immunofluorescence of SYCP3 (red) with either SMC3, SMC1α, SMC1β, RAD21, REC8 or STAG3 (green) in wild-type or *Rad21l*$^{-/-}$ spermatocytes. In wild-type pachytene spermatocytes, the cohesins SMC3 (**B**), SMC1α (**D**), SMC1β (**J**), RAD21 (**L**), REC8 (**R**) and STAG3 (**T**) colocalize with SYCP3 (**A, C, I, K, Q, S**) along the autosomal SCs and sex AEs with the exception of REC8 labelling at the XY bivalent, which is weaker in comparison with SYCP3. In *Rad21l*$^{-/-}$-arrested spermatocytes, the intensity and localization of the fluorescent signal corresponding to SMC3 (**F**), SMC1β (**N**), RAD21 (**P**) and REC8 (**V**) along the AE/LEs of the zygotene-like chromosomes is comparable to their wild-type controls and coincident with SYCP3 (**E, G, M, O, U**). However, the fluorescent signal of STAG3 (**X**) is notably decreased and absent in some regions where SYCP3 (**W**) labelling is present (arrows), whereas the intensity of the SMC1α (**H**) labelling is only partially reduced and delocalized. *Sex body (XY).

histological analysis of oocytes and ovarian sections. RAD21L has been localized to the AEs/LEs of the SC from early leptotene to pachytene, with loss of staining at later stages such as dictyate and metaphase I (Ishiguro *et al*, 2011). However, despite the fact that in oocytes the lack of RAD21L did not fully abolish synapsis as observed in spermatocytes and that fully synapsed bivalents were observed with a normal loading of STAG3 and SMC1α at their AE/LEs (Supplementary Figure S8A), a high proportion of the pachytene oocytes showed a slight defect in synapsis as determined by discontinuities in the labelling of SYCP3/SYCP1 at the synapsed LEs of the pachytene chromosomes ($69 \pm 4.3\%$ of cells in $Rad21l^{-/-}$ versus $12 \pm 3.6\%$ in wild type, $N = 30$, at 17.5 d.p.c. of age; Figure 8A). Chiasmata maintenance requires meiotic cohesion from yeast to mammals (Buonomo *et al*, 2000; Hodges *et al*, 2005). The cohesin-dependent mechanism for stabilizing sites of CO and centromeric cohesion is altered in an age-dependent manner
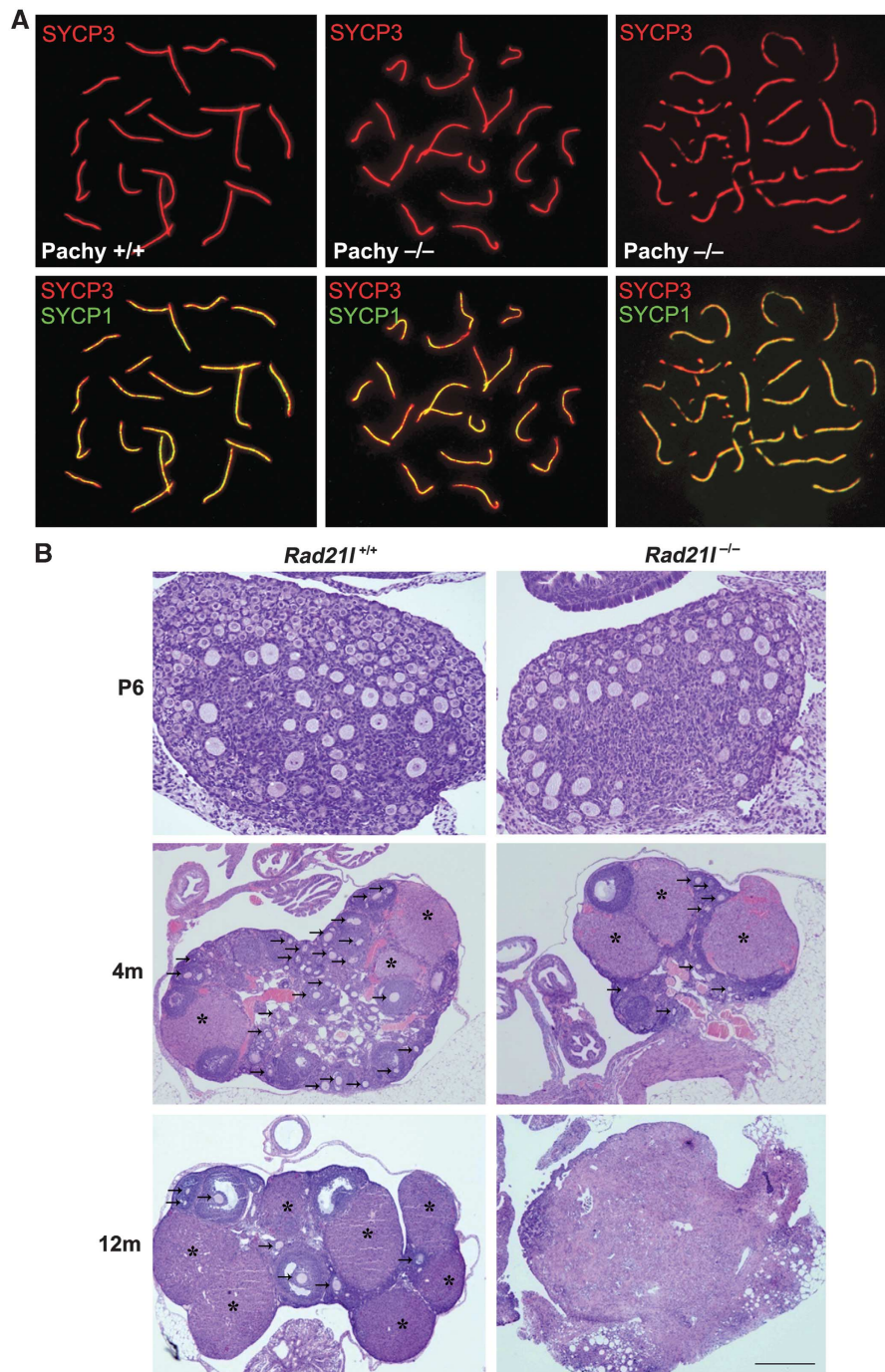

Figure 8 Female meiosis. (**A**) Double immunolabelling of SYCP3 (red) and SYCP1 (green) in pachytene oocytes from wild-type and mutant females showing normal (middle) and abnormal pairing (right). (**B**) Ovaries from RAD21L-deficient mice show atrophy with fibrosis and depletion of follicles. Comparative histological analysis of ovaries from $Rad21l^{-/-}$ and wild-type mice at 6 days (P6), 4 months (4 m) and 12 months (12 m) of age. Arrows indicate follicles and asterisks *corpora lutea*. Bar represents 500 μm in 4 m and 12 m, and 100 μm in P6.

leading to chromosome missegregation and aneuploidy (Hodges *et al*, 2005; Revenkova *et al*, 2010). Diakinesis/ metaphase I chromosomes from RAD21L-deficient oocytes were normal and 20 bivalents were always observed (Supplementary Figure S8B), indicating that RAD21L is not involved in chromosome cohesion during female meiosis. Taken together, these results suggest that a cohesion defect was not the underlying cause of the age-dependent infertility (Hodges *et al*, 2005; Chiang *et al*, 2010; Lister *et al*, 2010). Next, we comparatively studied the histology of ovaries from 12-month-old wild-type and mutant female mice and observed remarkable differences. While control ovaries showed more than five follicles at different stages of folliculogenesis and several *corpora lutea*, mutant ovaries displayed atrophy with a complete loss of primordial follicles (Figure 8B). In 4-month-old mice, the mutant ovaries presented a reduced number of follicles but a similar number of *corpora lutea* as wild-type littermates (Figure 8B). Thus, the ratio between the numbers of follicles and the numbers of *corpora lutea* is reduced in the *Rad21l*$^{-/-}$ when compared with controls. To further delineate at which stage during development this reduction is achieved, we histologically analysed ovaries from 6-day-old females (P6), a time point at which all oocytes are already arrested in dictyate (Peters, 1969). A four-fold decrease (4.1 ± 0.6, $N = 4$) in the number of small oocytes in the outer cortex where primordial follicles occur was found in *Rad21l*$^{-/-}$ compared with *Rad21l*$^{+/+}$. However, no substantial differences in the numbers of growing oocytes in the preantral stage of follicle development, which occupy the inner part of the cortex, were observed (Figure 8B; Peters, 1969). This demonstrates that young mutant females are able to ovulate physiologically in a similar way as the controls, and predicts that females will exhaust their pool of oocytes earlier than their wild-type counterparts leading to premature infertility.

In terms of human disease, this pathology resembles premature ovarian failure and its aetiology includes a strong genetic component (Shelling, 2010). In addition, women who suffer from ovarian failure after cancer chemotherapy or older healthy women also demonstrate a strikingly similar atrophy of the ovaries as we here observed in *Rad21l*$^{-/-}$ female mice (Meirow *et al*, 2007).

Sexual dimorphism in fertility in mouse mutants

Defects in early stages of the meiotic prophase I are common in several mouse mutants where meiotic genes have been ablated, these include *Spo11*, *Sycp3*, *Sycp2*, *Fkbp6* and *Trip13* (Baudat *et al*, 2000; Yuan *et al*, 2000; Crackower *et al*, 2003; Yang *et al*, 2006; Li and Schimenti, 2007). *Smc1β* and *Rec8* null mice are the only cohesin-deficient mice analysed meiotically and are infertile, while *Rad21* null mice are not viable (Xu *et al*, 2010). REC8-deficient mice fail to maintain inter-homologous synapsis, which leads to meiotic arrest in both genders (Bannister *et al*, 2004; Xu *et al*, 2005). *Smc1β* mutant mice show an arrest in pachytene stage in males, whereas females have weaker synapsis defect allowing progression up to the second division but they show unjoined chromatids due to a loss of centromeric cohesion (Revenkova *et al*, 2004). The RAD21L-deficient males generated and analysed in the present study reveal a phenotype as severe as the one observed in the *Rec8* mutant male mice, which also show a zygotene-like arrest. However, the subfertility of the RAD21L-deficient females is much milder than in SMC1β and REC8

female mice (Bannister *et al*, 2004; Revenkova *et al*, 2004; Xu *et al*, 2005).

Sexual dimorphism in meiotic genes has been previously observed in SYCP3 and SYCP2 mutant mice, where males are infertile whereas females are only subfertile (Yuan *et al*, 2000, 2002; Yang *et al*, 2006). This dimorphism has been attributed to a very weak synapsis surveillance mechanism and a reduced stringency of the spindle assemble checkpoint in oocytes in comparison to spermatocytes (Hunt and Hassold, 2002; Nagaoka *et al*, 2011), but this can also be explained by the prolonged prophase arrest following bivalent formation, which lasts from birth until ovulation. After this long-term arrest of oocytes at dictyate, most of the components of the former AEs/LEs of the disassembled SC do not remain/ relocate to the centromere or to the interchromatid domain of the bivalents at the next metaphase I. For instance, SYCP3, SYCP2 and RAD21 have been localized at the AEs/LEs of the SC during both male and female mouse meiosis, and also at the centromeres of metaphase I bivalents in spermatocytes (Offenberg *et al*, 1998; Parra *et al*, 2004; Ishiguro *et al*, 2011) but not in oocytes (Hodges *et al*, 2001; Tachibana-Konwalski *et al*, 2010). Likewise, RAD21L disappears from the AEs/LEs at dictyate and never labels the centromeres of metaphase I bivalents in oocytes (Ishiguro *et al*, 2011). In agreement with this, RAD21L-deficient females do not show premature loss of cohesion at metaphase I (20 bivalents are observed; Supplementary Figure S8B) and are therefore fertile. Thus, it can be speculated that mutations in this set of proteins (SYCP2, Yang *et al*, 2006; SYCP3, Yuan *et al*, 2000; Yuan *et al*, 2002; and RAD21L, this study), yield male infertility and female subfertility not only because of differences in the checkpoints between genders, but also because these proteins are not part of the segregation machinery of the chromosomes during female meiosis. This difference between male and female meiosis might contribute to the vulnerability of the female meiotic process by increasing the likelihood of premature sister chromatid separation.

From the spermatogenic point of view, it has been claimed that the meiotic sex chromosome inactivation (MSCI) that takes place in the sex bivalent in mid-pachytene spermatocytes can underlie the dimorphic infertility of several mouse mutants with a common type IV meiotic arrest (Barchi *et al*, 2005; Mahadevaiah *et al*, 2008). Recently, it has been elucidated that when MSCI fails at mid-pachytene, two pro-apoptotic transcription factors located at the Y chromosome (ZFY1/2) drive pachytene-arrested spermatocytes into a programmed cell death (Royo *et al*, 2010). We postulate that these same genes could also lead to the apoptosis observed in other mouse mutants with a developmental stage IV arrest, which are blocked well before MSCI take place at mid-pachytene. For instance, both DMC1- and SPO11-deficient spermatocytes arrest at developmental stage IV and their spermatocytes show similar level of apoptosis; however, their arrest corresponds to zygotene and to a mid-pachytene prophase, respectively (Yoshida *et al*, 1998; Baudat *et al*, 2000). Thus, we believe that the activation of the apoptotic programme in zygotene-like-arrested mutants, such as *Rad21l*$^{-/-}$ spermatocytes, can be caused by the expression of these and/or other unidentified pro-apoptotic genes for an indefinite lapse of time during the zygotene-like arrest.

Finally, it has been highlighted that the sexual dimorphism in fertility is dependent on those proteins that affect the

organization of the AEs/chromatin of the male XY bivalent (Kolas *et al*, 2005). This observation is also consistent with RAD21L playing a specific role in the pairing and the development of the sex body.

In yeast and vertebrates, a dual model of the ring closure of the cohesin complex by the kleisins REC8/RAD21 has long been accepted (Klein *et al*, 1999; Sonoda *et al*, 2001; Kudo *et al*, 2006; Tachibana-Konwalski *et al*, 2010). This model has been challenged by the existence of three meiosis-specific paralogues of the α-kleisins family of proteins in *C. elegans* (REC8, COH3, COH4). Similarly in mammals, the observed severity and penetrance of the phenotype in mice lacking RAD21L is comparable to the genetic ablation of the canonical meiotic kleisin REC8 in mouse spermatogenesis (Bannister *et al*, 2004; Xu *et al*, 2005), further demonstrating that these kleisins are not redundant and are similarly important in male meiotic prophase. Overall, these results provide *in vivo* evidence for the functional relevance of the α-kleisin RAD21L in SC assembly, homologous recombination, and synapsis during mammalian meiosis and suggest a re-examination of the contribution of the α-kleisin paralogues in mammalian meiosis.

Materials and methods

Immunocytology
Testes were detunicated and processed for spreading using a conventional 'dry-down' technique or squashing (Parra *et al*, 2004). Oocytes from fetal ovaries (E17.5 embryos) were digested with collagenase, incubated in hypotonic buffer, disaggregated, fixed in paraformaldehyde and incubated with the indicated antibodies for immunofluorescence (see Supplementary data). Both polyclonal antibodies against RAD21L (Gutiérrez-Caballero *et al*, 2011) were used indistinctly for the IF and western blot data presented throughout this work. In all the cases, the results were validated with both antibodies.

Mice
We developed a non-conditional mutant mouse by standard gene targeting methods using an insertional strategy. Briefly, two homology arms separated apart by a gap were PCR amplified from a BAC clone enclosing RAD21L and cloned into the plasmid p5'HPRT (Adams *et al*, 2004). The targeting vector was linearized at a new restriction site generated between both ends flanking the gap, and electroporated in ES cells following standard procedures (see Supplementary data). The genetic background under which the mutation was analysed is a mixed BL6/129. The handling, maintenance and care of the animals, as well as all procedures performed in this study, were in accordance with the institutional guidelines (CSIC and USAL). $Rad21l^{+/-}$ and $Rad21l^{+/+}$ were used as controls in all the experiments throughout the study. To simplify, we only show the $Rad21l^{+/+}$ and $Rad21l^{-/-}$ results.

FACS analysis
Wild-type, $Rad21l^{+/-}$ and $Rad21l^{-/-}$ testicular cells preparation and their DNA content measurement were performed by a standard procedure (Kudo *et al*, 2009).

OA assay
Testes from wild-type and $Rad21l^{-/-}$ were detunicated and cultured as previously described (Revenkova *et al*, 2004). Briefly, 5×10^6 cell/ml were plated in $35 \times 10 \, \text{mm}^2$ culture dishes containing complete culture medium supplemented with 25 mM HEPES. Cells were cultured at $32\,^{\circ}\text{C}$ for 5–6 h with $5\,\mu\text{M}$ OA (Sigma-Aldrich). Spreading and immunofluorescence were performed as previously mentioned.

Telomeric analysis
Squashed tubules were double immunolabelled with SYCP3 and RAP1. For each nucleus, partial *Z* projections of the top, equator and bottom portions were captured using an Olympus DP70 digital camera controlled by AnalySIS software (Soft Imaging System). All projections result from the superimposition of 15 focal planes throughout a certain nuclear region.

Histology
For adult male histological analysis, mice were perfused and their testes/ovaries were processed into serial paraffin sections and stained with haematoxylin–eosin. For TUNEL assay, sections were deparaffinized and apoptotic cells were detected with the *In Situ* Cell Death Detection Kit (Roche) and counterstained with DAPI. Apoptotic cells were pseudocoloured in green. Immunohistochemical detection of proliferating cells with α-PCNA ab29 (1:200, Abcam) involved antigen retrieval with citrate buffer at pH 6.0. For histological studies of 13 and 19 days mice, testes were fixed in Bouin's fixative.

Giemsa staining of diakinesis-stage mouse oocytes
To analyse crossovers at diakinesis, we did chromosome preparations of oocytes ($n \geqslant 15$ per female) from three females of 18 weeks of age from each genotype following the method described previously (Kan *et al*, 2008).

Supplementary data
Supplementary data are available at *The EMBO Journal* Online (http://www.embojournal.org).

Conflict of interest

The authors declare that they have no conflict of interest.

References

Adams DJ, Biggs PJ, Cox T, Davies R, van der Weyden L, Jonkers J, Smith J, Plumb B, Taylor R, Nishijima I, Yu Y, Rogers J, Bradley A (2004) Mutagenic insertion and chromosome engineering resource (MICER). *Nat Genet* **36:** 867–871

Adelfalk C, Janschek J, Revenkova E, Blei C, Liebe B, Göb E, Alsheimer M, Benavente R, de Boer E, Novak I, Höög C, Scherthan H, Jessberger R (2009) Cohesin SMC1beta protects telomeres in meiocytes. *J Cell Biol* **187:** 185–199

Bannister LA, Reinholdt LG, Munroe RJ, Schimenti JC (2004) Positional cloning and characterization of mouse *mei8*, a disrupted allele of the meiotic cohesin Rec8. *Genesis* **40:** 184–194

Barchi M, Mahadevaiah S, Di Giacomo M, Baudat F, de Rooij DG, Burgoyne PS, Jasin M, Keeney S (2005) Surveillance of different recombination defects in mouse spermatocytes yields distinct responses despite elimination at an identical developmental stage. *Mol Cell Biol* **25:** 7203–7215

Baudat F, Manova K, Yuen JP, Jasin M, Keeney S (2000) Chromosome synapsis defects and sexually dimorphic meiotic progression in mice lacking Spo11. *Mol Cell* **6:** 989–998

Buonomo SB, Clyne RK, Fuchs J, Loidl J, Uhlmann F, Nasmyth K (2000) Disjunction of homologous chromosomes in meiosis I depends on proteolytic cleavage of the meiotic cohesin Rec8 by separin. *Cell* **103:** 387–398

Chiang T, Duncan FE, Schindler K, Schultz RM, Lampson MA (2010) Evidence that weakened centromere cohesin is a leading cause of age-related aneuploidy in oocytes. *Curr Biol* **20:** 1522–1528

Crackower MA, Kolas NK, Noguchi J, Sarao R, Kikuchi K, Kaneko H, Kobayashi E, Kawai Y, Kozieradzki I, Landers R, Mo R, Hui CC, Nieves E, Cohen PE, Osborne LR, Wada T, Kunieda T, Moens PB, Penninger JM (2003) Essential role of Fkbp6 in male fertility and homologous chromosome pairing in meiosis. *Science* **300:** 1291–1295

Eijpe M, Offenberg H, Jessberger R, Revenkova E, Heyting C (2003) Meiotic cohesin REC8 marks the axial elements of rat synaptonemal complexes before cohesins SMC1beta and SMC3. *J Cell Biol* **160:** 657–670

Gómez R, Valdeolmillos A, Parra MT, Viera A, Carreiro C, Roncal F, Rufas JS, Barbero JL, Suja JA (2007) Mammalian SGO2 appears at the inner centromere domain and redistributes depending on tension across centromeres during meiosis II and mitosis. *EMBO Rep* **8:** 173–180

Gruber S, Haering CH, Nasmyth K (2003) Chromosomal cohesin forms a ring. *Cell* **112:** 765–777

Gutiérrez-Caballero C, Herrán Y, Sánchez-Martín MS, Suja JA, Barbero JL, Llano E, Pendás AM (2011) Identification and molecular characterization of the mammalian kleisin RAD21L. *Cell Cycle* **10:** 1477–1487

Hartsuiker E, Vaessen E, Carr AM, Kohli J (2001) Fission yeast Rad50 stimulates sister chromatid recombination and links cohesion with repair. *EMBO J* **20:** 6660–6671

Henderson KA, Keeney S (2005) Synaptonemal complex formation: where does it start? *Bioessays* **7:** 995–998

Hodges CA, LeMaire-Adkins R, Hunt PA (2001) Coordinating the segregation of sister chromatids during the first meiotic division: evidence for sexual dimorphism. *J Cell Sci* **114:** 2417–2426

Hodges CA, Revenkova E, Jessberger R, Hassold TJ, Hunt PA (2005) SMC1beta-deficient female mice provide evidence that cohesins are a missing link in age-related nondisjunction. *Nat Genet* **37:** 1351–1355

Hunt PA, Hassold TJ (2002) Sex matters in meiosis. *Science* **296:** 2181–2183

Ishiguro KI, Kim J, Fujiyama-Nakamura S, Kato S, Watanabe Y (2011) A new meiosis-specific cohesin complex implicated in the cohesin code for homologous pairing. *EMBO Rep* **12:** 267–275

Kan R, Sun X, Kolas NK, Avdievich E, Kneitz B, Edelmann W, Cohen PE (2008) Comparative analysis of meiotic progression in female mice bearing mutations in genes of the DNA mismatch repair pathway. *Biol Reprod* **78:** 462–471

Klein F, Mahr P, Galova M, Buonomo SB, Michaelis C, Nairz K, Nasmyth K (1999) A central role for cohesins in sister chromatid cohesion, formation of axial elements, and recombination during yeast meiosis. *Cell* **98:** 91–103

Kolas NK, Marcon E, Crackower MA, Höög C, Penninger JM, Spyropoulos B, Moens PB (2005) Mutant meiotic chromosome core components in mice can cause apparent sexual dimorphic endpoints at prophase or X-Y defective male-specific sterility. *Chromosoma* **114:** 92–102

Kudo NR, Anger M, Peters AH, Stemmann O, Theussl HC, Helmhart W, Kudo H, Heyting C, Nasmyth K (2009) Role of cleavage by separase of the Rec8 kleisin subunit of cohesin during mammalian meiosis I. *J Cell Sci* **122:** 2686–2698

Kudo NR, Wassmann K, Anger M, Schuh M, Wirth KG, Xu H, Helmhart W, Kudo H, McKay M, Maro B, Ellenberg J, de Boer P, Nasmyth K (2006) Resolution of chiasmata in oocytes requires separase-mediated proteolysis. *Cell* **126:** 135–146

Lee J, Hirano T (2011) RAD21L, a novel cohesin subunit implicated in linking homologous chromosomes in mammalian meiosis. *J Cell Biol* **192:** 263–276

Li XC, Schimenti JC (2007) Mouse pachytene checkpoint 2 (trip13) is required for completing meiotic recombination but not synapsis. *PLoS Genet* **3:** e130

Lister L, Kouznetsova A, Hyslop L, Kalleas D, Pace S, Barel J, Nathan A, Floros V, Adelfalk C, Watanabe Y, Jessberger R, Kirkwood TB, Höög C, Herbert M (2010) Age-related meiotic segregation errors in mammalian oocytes are preceded by depletion of cohesin and Sgo2. *Curr Biol* **20:** 1511–1521

Llano E, Gómez R, Gutiérrez-Caballero C, Herrán Y, Sánchez-Martín M, Vázquez-Quiñones L, Hernández T, de Alava E, Cuadrado A, Barbero JL, Suja JA, Pendás AM (2008) Shugoshin-2 is essential for the completion of meiosis but not for mitotic cell division in mice. *Genes Dev* **22:** 2400–2413

Losada A, Hirano M, Hirano T (2002) Cohesin release is required for sister chromatid resolution, but not for condensin-mediated compaction, at the onset of mitosis. *Genes Dev* **16:** 3004–3016

Mahadevaiah SK, Bourc'his D, de Rooij DG, Bestor TH, Turner JM, Burgoyne PS (2008) Extensive meiotic asynapsis in mice antagonises meiotic silencing of unsynapsed chromatin and consequently disrupts meiotic sex chromosome inactivation. *J Cell Biol* **182:** 263–276

Meirow D, Dor J, Kaufman B, Shrim A, Rabinovici J, Schiff E, Raanani H, Levron J, Fridman E (2007) Cortical fibrosis and blood-vessels damage in human ovaries exposed to chemotherapy. Potential mechanisms of ovarian injury. *Hum Reprod* **22:** 1626–1633

Mimitou EP, Symington LS (2009) DNA end resection: many nucleases make light work. *DNA Repair* **8:** 983–995

Moens PB, Marcon E, Shore JS, Kochakpour N, Spyropoulos B (2007) Initiation and resolution of interhomolog connections: crossover and non-crossover sites along mouse synaptonemal complexes. *J Cell Sci* **120:** 1017–1027

Musacchio A, Salmon ED (2007) The spindle-assembly checkpoint in space and time. *Nat Rev Mol Cell Biol* **8:** 379–393

Nagaoka SI, Hodges CA, Albertini DF, Hunt PA (2011) Oocyte-specific differences in cell-cycle control create an innate susceptibility to meiotic errors. *Curr Biol* **26:** 651–657

Offenberg HH, Schalk JA, Meuwissen RL, van Aalderen M, Kester HA, Dietrich AJ, Heyting C (1998) SCP2: a major protein component of the axial elements of synaptonemal complexes of the rat. *Nucleic Acids Res* **26:** 2572–2579

Parisi S, McKay MJ, Molnar M, Thompson MA, van der Spek PJ, van Drunen-Schoenmaker E, Kanaar R, Lehmann E, Hoeijmakers JHJ, Kohli J (1999) Rec8p, a meiotic recombination and sister chromatid cohesion phosphoprotein of the Rad21p family conserved from fission yeast to humans. *Mol Cell Biol* **19:** 3515–3528

Parra MT, Gómez R, Viera A, Llano E, Pendás AM, Rufas JS, Suja JA (2009) Sequential assembly of centromeric proteins in male mouse meiosis. *PLoS Genet* **5:** e1000417

Parra MT, Gómez R, Viera A, Page J, Calvente A, Wordeman L, Rufas JS, Suja JA (2006) A perikinetochoric ring defined by MCAK and Aurora-B as a novel centromere domain. *PLoS Genet* **2:** e84

Parra MT, Viera A, Gómez R, Page J, Benavente R, Santos JL, Rufas JS, Suja JA (2004) Involvement of the cohesin Rad21 and SCP3 in monopolar attachment of sister kinetochores during mouse meiosis I. *J Cell Sci* **117:** 1221–1234

Perera D, Perez-Hidalgo L, Moens PB, Reini K, Lakin N, Syväoja JE, San-Segundo PA, Freire R (2004) TopBP1 and ATR colocalization at meiotic chromosomes: role of TopBP1/Cut5 in the meiotic recombination checkpoint. *Mol Biol Cell* **15:** 1568–1579

Peters H (1969) The development of the mouse ovary from birth to maturity. *Acta Endocrinol (Copenh)* **62:** 98–116

Prieto I, Suja JA, Pezzi N, Kremer L, Martínez-A C, Rufas JS, Barbero JL (2001) Mammalian STAG3 is a cohesin specific to sister chromatid arms in meiosis I. *Nat Cell Biol* **3:** 761–766

Revenkova E, Eijpe M, Heyting C, Hodges CA, Hunt PA, Liebe B, Scherthan H, Jessberger R (2004) Cohesin SMC1 beta is required for meiotic chromosome dynamics, sister chromatid cohesion and DNA recombination. *Nat Cell Biol* **6:** 555–562

Revenkova E, Herrmann K, Adelfalk C, Jessberger R (2010) Oocyte cohesin expression restricted to pre-dictyate stages provides full fertility and prevents aneuploidy. *Curr Biol* **20:** 1529–1533

Royo H, Polikiewicz G, Mahadevaiah SK, Prosser H, Mitchell M, Bradley A, de Rooij DG, Burgoyne PS, Turner JM (2010) Evidence that meiotic sex chromosome inactivation is essential for male fertility. *Curr Biol* **20:** 2117–2123

Russell LD (1990) *Histological and Histopathological Evaluation of the Testis.* 1st edn. Cache River Press, Quick Publishing: St Louis, MO

Santucci-Darmanin S, Walpita D, Lespinasse F, Desnuelle C, Ashley T, Paquis-Flucklinger V (2000) MSH4 acts in conjunction with MLH1 during mammalian meiosis. *FASEB J* **11:** 1539–1547

Scherthan H (2001) A bouquet makes ends meet. *Nat Rev Mol Cell Biol* **2:** 621–627

Severson AF, Ling L, van Zuylen V, Meyer BJ (2009) The axial element protein HTP-3 promotes cohesin loading and meiotic axis assembly in C. elegans to implement the meiotic program of chromosome segregation. *Genes Dev* **23:** 1763–1778

Shelling AN (2010) Premature ovarian failure. *Reproduction* **140:** 633–641

Sonoda E, Matsusaka T, Morrison C, Vagnarelli P, Hoshi O, Ushiki T, Nojima K, Fukagawa T, Waizenegger IC, Peters JM, Earnshaw WC, Takeda S (2001) Scc1/Rad21/Mcd1 is required for sister chromatid cohesion and kinetochore function in vertebrate cells. *Dev Cell* **6:** 759–770

Suja JA, Barbero JL (2009) Cohesin complexes and sister chromatid cohesion in mammalian meiosis. *Genome Dyn* **5:** 94–116

Sumara I, Vorlaufer E, Stukenberg PT, Kelm O, Redemann N, Nigg EA, Peters JM (2002) The dissociation of cohesin from chromosomes in prophase is regulated by Polo-like kinase. *Mol Cell* **9:** 515–525

Tachibana-Konwalski K, Godwin J, van der Weyden L, Champion L, Kudo NR, Adams DJ, Nasmyth K (2010) Rec8-containing cohesin maintains bivalents without turnover during the growing phase of mouse oocytes. *Genes Dev* **24:** 2505–2516

Viera A, Rufas JS, Martínez I, Barbero JL, Ortega S, Suja JA (2009) CDK2 is required for proper homologous pairing, recombination

and sex-body formation during male mouse meiosis. *J Cell Sci* **122:** 2149–2159

Wiltshire T, Park C, Caldwell KA, Handel MA (1995) Induced premature G2/M-phase transition in pachytene spermatocytes includes events unique to meiosis. *Dev Biol* **169:** 557–567

Xu H, Balakrishnan K, Malaterre J, Beasley M, Yan Y, Essers J, Appeldoorn E, Tomaszewski JM, Vazquez M, Verschoor S, Lavin MF, Bertoncello I, Ramsay RG, McKay MJ (2010) Rad21-cohesin haploinsufficiency impedes DNA repair and enhances gastrointestinal radiosensitivity in mice. *PLoS One* **5:** e12112

Xu H, Beasley MD, Warren WD, van der Horst GT, McKay MJ (2005) Absence of mouse REC8 cohesin promotes synapsis of sister chromatids in meiosis. *Dev Cell* **8:** 949–961

Yang F, De La Fuente R, Leu NA, Baumann C, McLaughlin KJ, Wang PJ (2006) Mouse SYCP2 is required for synaptonemal complex assembly and chromosomal synapsis during male meiosis. *J Cell Biol* **173:** 497–507

Yoshida K, Kondoh G, Matsuda Y, Habu T, Nishimune Y, Morita T (1998) The mouse RecA-like gene Dmc1 is required for homologous chromosome synapsis during meiosis. *Mol Cell* **1:** 707–718

Yuan L, Liu JG, Hoja MR, Wilbertz J, Nordqvist K, Höög C (2002) Female germ cell aneuploidy and embryo death in mice lacking the meiosis-specific protein SCP3. *Science* **296:** 1115–1118

Yuan L, Liu JG, Zhao J, Brundell E, Daneholt B, Hoog C (2000) The murine SCP3 gene is required for synaptonemal complex assembly, chromosome synapsis, and male fertility. *Mol Cell* **5:** 73–83